

Bi-cLSTM: Residual-Corrected Bidirectional LSTM for Aero-Engine RUL Estimation

Rafi Hassan Chowdhury¹, Nabil Daiyan³, Faria Ahmed¹, Md Redwan Iqbal⁴, Morsalin Sheikh⁴

²Department of Computer Science and Engineering, Islamic University of Technology, Gazipur 1704, Bangladesh
{rafihassan, fariaahmed}@iut-dhaka.edu

³Department of Computer Science and Engineering, Rajshahi University of Engineering and Technology, Rajshahi, Bangladesh
1803014@student.ruet.ac.bd

⁴Department of Aeronautical Engineering, Military Institute of Science and Technology, Dhaka 1216, Bangladesh
{redwan400900, morsalin.ae.mist}@gmail.com

Abstract—Accurate Remaining Useful Life (RUL) prediction is a key requirement for effective Prognostics and Health Management (PHM) in safety-critical systems such as aero-engines. Existing deep learning approaches, particularly LSTM-based models, often struggle to generalize across varying operating conditions and are sensitive to noise in multivariate sensor data. To address these challenges, we propose a novel Bidirectional Residual Corrected LSTM (Bi-cLSTM) model for robust RUL estimation. The proposed architecture combines bidirectional temporal modeling with an adaptive residual correction mechanism to iteratively refine sequence representations. In addition, we introduce a condition-aware preprocessing pipeline incorporating regime-based normalization, feature selection, and exponential smoothing to improve robustness under complex operating environments. Extensive experiments on all four subsets of the NASA C-MAPSS dataset demonstrate that the proposed Bi-cLSTM consistently outperforms LSTM-based baselines and achieves competitive state-of-the-art performance, particularly on challenging multi-condition scenarios. These results highlight the effectiveness of combining bidirectional temporal learning with residual correction for reliable RUL prediction.

Index Terms—Bi-cLSTM, Sensor Data, C-MAPSS, Degradation Modeling, RUL Estimation

I. INTRODUCTION

The commercial aerospace sector has a global industry of \$ 1.5 trillion. 40% of airline maintenance expenses are spent on engine maintenance [1]. Although aircraft engines rarely shut down, the operational and financial consequences are very high. Accurately estimating the RUL earlier helps operators act proactively rather than reflectively. In this way, we can reduce unplanned downtime and operational costs.

Recent advances in deep learning have substantially improved the prediction of Remaining Useful Life (RUL). Asif et al. [2] proposed a deep learning model using the C-MAPSS dataset. This work is focused on turbofan engine RUL prediction and achieves accuracy improvement through effective spatiotemporal feature extraction and computational efficiency. Zhang et al. [3] introduced a deep equilibrium model with iterative fixed-point computation. It shows better results in estimating complex temporal degradation patterns, but higher computational demands. Liu et al. presented an optimized

predictive framework enhanced accuracy but lacked explicit techniques for noise and redundancy mitigation [4]. Hong et al. combined explainability with dimensionality reduction to increase model interpretability, though this sometimes sacrificed information and increased computational overhead [5].

Despite considerable progress, many existing RUL models based on classical machine learning and deep neural networks, including LSTM and hybrid models, face challenges such as overfitting, sensitivity to noise [2], and limited generalization to varied operating conditions [3], [4].

We introduce an enhanced Bidirectional Corrected LSTM (Bi_cLSTM) for robust Remaining Useful Life (RUL) prediction. The model integrates bidirectional temporal modeling with a residual correction mechanism to refine predictions at each step. A preprocessing pipeline including condition aware normalization, Random Forest feature selection, and exponential smoothing reduces noise and redundancy. On the C-MAPSS dataset, Bi-cLSTM surpasses LSTM, cLSTM, and Bi-LSTM baselines, achieving lower RMSE and higher R², particularly on the challenging FD002 and FD004 subsets, demonstrating its ability to capture long-range temporal and contextual dependencies in complex operating conditions. [6]–[14]

The remainder of this paper reviews related work, discusses a detailed proposed methodology, presents comprehensive experimental results and comparative analyses, and concludes with key findings, limitations, and future research directions.

II. METHODOLOGY

A. Dataset

We experimented on the Commercial Modular Aero-Propulsion System Simulation (C-MAPSS) dataset [15], a widely used benchmark for Remaining Useful Life (RUL) prediction, provided by NASA's Prognostics Center of Excellence. The dataset simulates turbofan engine degradation under various operating conditions and fault modes, with 21 sensor signals (e.g., temperatures, pressures, rotational speeds) and three different operational settings. The task is to predict RUL based on these sensor measurements.

TABLE I: Each Sub-Unit of the C-MAPSS Dataset

Dataset	FD001	FD002	FD003	FD004
Engines in training set	100	260	100	249
Engines in testing set	100	259	100	248
Training trajectories	17,731	48,558	21,120	56,815
Testing trajectories	100	259	100	248
Max/min cycle for train	362/128	378/128	525/145	543/128
Max/min cycle for test	303/31	367/21	475/38	486/19
Operating Conditions	1	6	1	6
Fault Modes	1	1	2	2

The dataset is of four subsets: FD001, FD002, FD003, and FD004, each have different levels of complexity. FD001 and FD003 have simpler configurations with one operating condition, on the other hand FD002 and FD004 include multiple conditions and fault modes. The number of engines and testing trajectories vary across subsets, as detailed in Table I. Sensor signals are normalized, and the maximum RUL is capped at 125 cycles to avoid bias from early stable phases.

Output parameters, such as fan speed, pressure, and temperature are summarized in Table II. To ensure robust evaluation, the training and validation sets for each subset are split without any overlap with the test set, following established protocols to avoid data leakage.

B. Dataset Preprocessing

We utilized the NASA C-MAPSS turbofan engine degradation dataset, which provides multivariate time-series sensor measurements from engines operated until failure. Each record includes an engine identifier, a cycle index, three operational settings, and twenty-one sensor channels. The Remaining Useful Life (RUL) was defined as the number of cycles left until failure, computed as

$$RUL_{i,t} = \max(0, T_i - t), \quad (1)$$

where T_i is the final cycle of engine i . For the test set, the provided offsets were incorporated into the terminal RUL values. To reduce extreme variations and improve model stability, all RUL values were clipped at 125 cycles following the standard practice in prognostics studies [16].

Normalization was performed to account for distributional differences across operating conditions. For single-condition subsets (FD001 and FD003), a global z-score standardization was applied to all sensor channels:

$$z = \frac{x - \mu}{\sigma}, \quad (2)$$

where μ and σ are computed from the training set. For multi-condition subsets (FD002 and FD004), the three operational settings ($os1$, $os2$, $os3$) were clustered into six regimes using K-means, and regime-specific normalization was applied within each cluster. The operational settings themselves were globally standardized to ensure consistency across engines.

To reduce redundancy, a Random Forest Regressor was used for feature selection. Sensors with importance scores below 10^{-3} were removed, leaving only the most informative

TABLE II: Output Parameters of the C-MAPSS Turbofan Engine Datasets

Sensor Parameter	Description with Units
T2	Total Temperature in fan inlet (°R)
T24	Total Temperature at LPC outlet (°R)
T30	Total Temperature at HPC outlet (°R)
T50	Total Temperature at LPT outlet (°R)
P2	Pressure at fan inlet (psia)
P15	Total pressure in bypass-duct (psia)
P30	Total pressure at HPC outlet (psia)
Nf	Physical fan speed (rpm)
Nc	Physical core speed (rpm)
Epr	Engine pressure ratio (-)
Ps30	Static pressure at HPC outlet (psia)
Phi	Ratio of fuel flow to Ps30 (psi)
NRf	Corrected fan speed (rpm)
Nrc	Corrected core speed (rpm)
BPR	Bypass ratio (-)
farB	Burner fuel air ratio (-)
htBleed	Bleed enthalpy (-)
NF-dmd	Demanded fan speed (rpm)
PCNR-dmd	Demanded corrected fan speed (rpm)
W31	HPT coolant bleed (lbm/s)
W32	LPT coolant bleed (lbm/s)

variables. In addition, sensor measurements were smoothed using an exponentially weighted moving average (EWMA):

$$\hat{x}_t = \beta \hat{x}_{t-1} + (1 - \beta)x_t, \quad (3)$$

with a smoothing factor $\beta = 0.98$. Both raw and smoothed features were retained to capture short-term fluctuations as well as long-term degradation trends.

Sequential inputs were constructed using a sliding-window approach. Each subsequence comprised $W = 15$ consecutive cycles, and the label was defined as the RUL at the final cycle of the window. Early cycles with $t \leq 10$ were excluded to avoid unstable initialization effects. For evaluation, only the final subsequence from each test unit was retained. The dataset was split into 80% training and 20% validation sets. The final input tensors were structured as

$$\mathbf{X} \in \mathbb{R}^{B \times W \times F}, \quad (4)$$

where B is the batch size, $W = 15$ is the sequence length, and F is the number of selected features.

C. Corrector Module

The **Corrector** module is a residual correction mechanism designed to refine the outputs of sequential models, such as LSTMs and Bi-LSTMs, by learning an adaptive correction vector at each time step. This correction vector \mathbf{C}_t is added to the model's hidden state \mathbf{h}_t to improve prediction accuracy, particularly in tasks with noisy or incomplete data. The corrected output is given by:

$$\mathbf{h}_t^{\text{corrected}} = \text{LayerNorm}(\mathbf{h}_t + \mathbf{C}_t) \quad (5)$$

where $\mathbf{C}_t = f(\mathbf{h}_t, \mathbf{x}_t)$ is the correction term computed by a small feedforward network, and LayerNorm ensures stability by normalizing the corrected output.

During training, the Corrector is integrated into the model, and its parameters are learned through backpropagation using

the same loss function as the overall network. The model minimizes the Mean Squared Error (MSE) between the corrected predictions and the true labels. The inclusion of the Corrector improves temporal feature refinement, mitigates the impact of noise, and stabilizes the training process, making it particularly effective for predictive tasks like Remaining Useful Life (RUL) estimation.

D. Proposed Bi-cLSTM (Bidirectional Corrected LSTM)

The Bi-cLSTM model integrates bidirectional LSTM networks with a residual correction mechanism to enhance the prediction accuracy of sequential tasks, such as Remaining Useful Life (RUL) estimation. The primary goal of the architecture is to capture complex temporal dependencies in sequential data, while the residual correction mechanism refines predictions at each time step, compensating for potential inaccuracies in the LSTM’s raw output.

The model starts by passing the input features $\mathbf{x}_t \in \mathbb{R}^d$ through a projection layer that maps the raw input into a higher-dimensional space. This transformation enables the model to learn richer representations of the input sequence, which allows it to better capture complex temporal relationships inherent in the data. The projection is defined as:

$$\mathbf{z}_t = \text{ReLU}(\mathbf{W}_p \mathbf{x}_t + \mathbf{b}_p)$$

where \mathbf{W}_p and \mathbf{b}_p are the projection matrix and bias term, respectively, and ReLU is a non-linear activation function that introduces non-linearity into the transformation. This non-linearity enables the model to better handle complex data patterns that are not linearly separable.

Following the projection, the sequence is processed by multiple bidirectional LSTM blocks. The bidirectional LSTM captures both past and future dependencies by processing the input sequence in both forward and backward directions. This bidirectional processing is essential for tasks where both historical and future context are equally important for accurate prediction. Each LSTM block learns the temporal dependencies at each time step, producing hidden states \mathbf{h}_t and cell states \mathbf{c}_t as follows:

$$\mathbf{h}_t, \mathbf{c}_t = \text{LSTM}(\mathbf{z}_t, \mathbf{h}_{t-1}, \mathbf{c}_{t-1})$$

After processing through the LSTM blocks, the output is passed to the Corrector module, which computes a correction term \mathbf{C}_t for each time step. This correction is added to the LSTM output to refine the predictions. The final output from each block is then concatenated, and the RUL prediction is made through a fully connected layer:

$$\hat{y}_t = \mathbf{W}_h \cdot \mathbf{h}_t^{\text{corrected}} + \mathbf{b}_h$$

The model is trained end-to-end using a Mean Squared Error (MSE) loss function, minimizing the difference between the predicted and true RUL values. Training is performed using backpropagation through time (BPTT) with the Adam optimizer, and early stopping is applied to prevent overfitting.

TABLE III: RUL prediction performance (RMSE, MAE in units; R^2 dimensionless) on FD001 Sub-Unit

Architecture	RMSE	MAE	R^2
LSTM	27.5375	0.1607	0.5276
cLSTM	18.9375	0.1089	0.7766
Bi-LSTM	20.2125	0.1194	0.7454
Bi-cLSTM	17.5125	0.1066	0.8089

TABLE IV: Bi_cLSTM ablation across number of blocks using RMSE (lower is better).

Dataset	2 Blocks	4 Blocks	6 Blocks	8 Blocks	10 Blocks
FD001	19.59	17.51	18.11	21.81	21.91
FD002	14.73	13.96	14.10	14.12	14.61
FD003	24.61	21.85	22.98	22.98	21.38
FD004	14.74	14.25	15.44	14.63	15.74

The parameters of the LSTM blocks and the Corrector module are updated jointly, allowing the model to learn both temporal dependencies and appropriate corrections during training.

III. RESULT ANALYSIS

A. Performance of different baseline architectures

The Table III presents the performance comparison of different architectures for Remaining Useful Life (RUL) prediction, evaluated using Root Mean Squared Error (RMSE), Mean Absolute Error (MAE), and R^2 metrics. Among the models evaluated, the Bi-cLSTM architecture outperforms the others in all three metrics, achieving the lowest RMSE, MAE, and the highest R^2 score. This demonstrates its superior ability to predict RUL with higher accuracy compared to the LSTM, cLSTM, and Bi-LSTM models.

The cLSTM and Bi-LSTM models show improvements over the basic LSTM, with cLSTM achieving the second-best results in terms of RMSE and MAE, as well as a high R^2 value. The Bi-LSTM, while performing better than the LSTM, still falls short of the Bi-cLSTM in all evaluated metrics, highlighting the effectiveness of incorporating the correction mechanism in the Bi-cLSTM model for improved RUL predictions.

B. Ablation Studies

Table IV presents the ablation results of our Bi-cLSTM model across different numbers of blocks, evaluated by RMSE. The results show that the model performs optimally with four blocks, achieving the lowest RMSE on FD001 (17.51), FD002 (13.96), and FD004 (14.25). Increasing the number of blocks beyond four does not significantly improve performance and, in some cases, leads to a slight deterioration in RMSE, particularly on FD001 and FD003.

For FD003, the best performance occurs with 10 blocks (RMSE 21.38), indicating that adding more blocks can be beneficial in more complex datasets with multiple fault modes. However, for simpler datasets like FD002, the addition of more blocks beyond four results in marginal gains, suggesting that our model already captures sufficient temporal dependencies with four blocks. Based on this ablation study, we selected four blocks as the optimal configuration for our model.

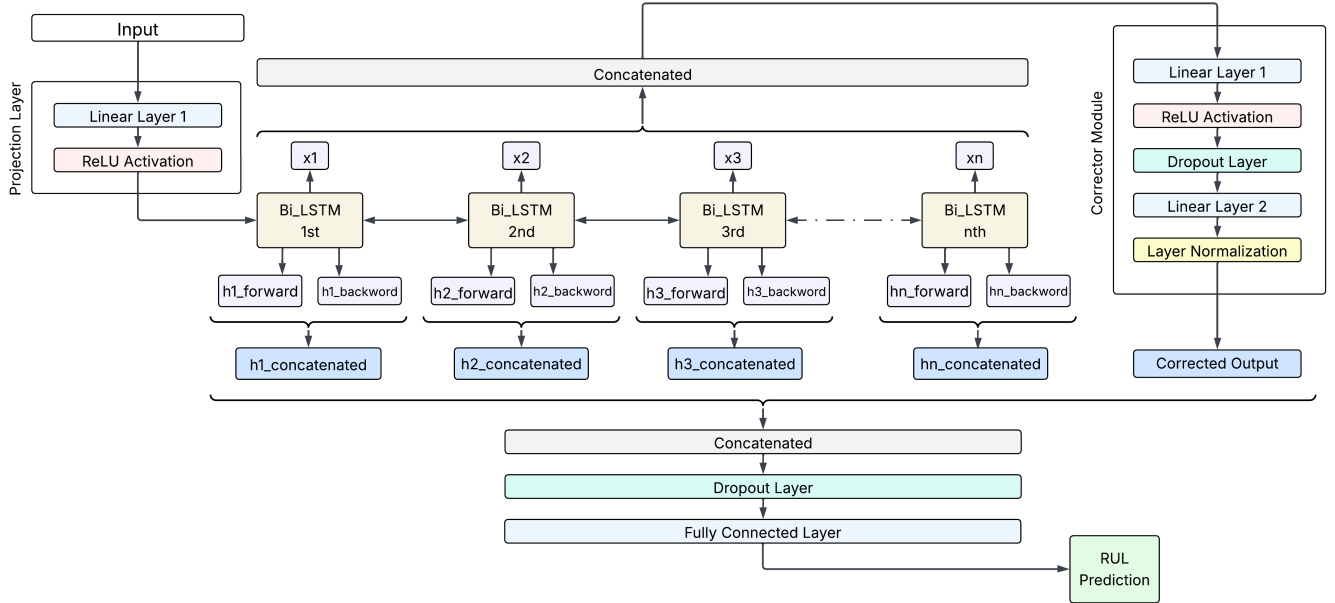


Fig. 1: Proposed Bi-cLSTM framework with a residual Corrector module. Input features are projected, processed by bidirectional LSTMs, refined through adaptive correction, and mapped to Remaining Useful Life (RUL) predictions.

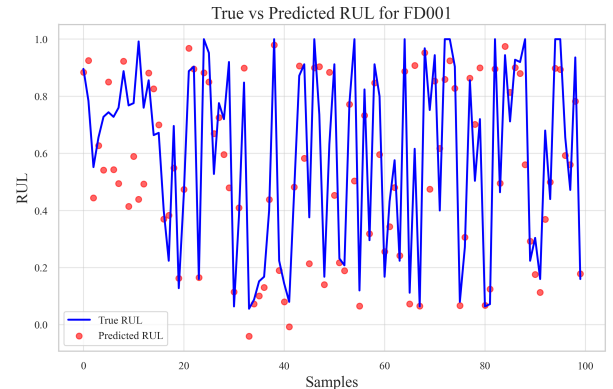
This ablation study demonstrates that while increasing the number of blocks improves performance on more challenging datasets, a smaller number of blocks is sufficient for simpler datasets, thus balancing efficiency and accuracy.

C. Comparison with State-of-the-Art Methods

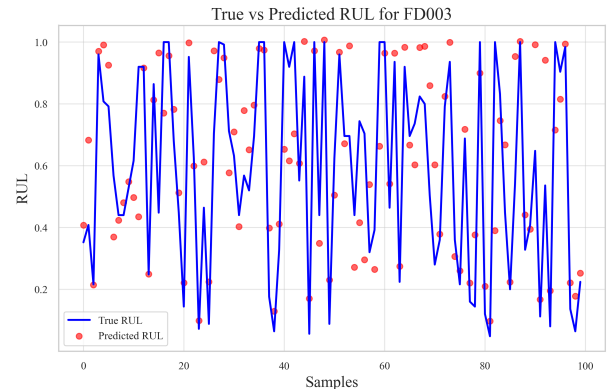
Table V presents a chronological comparison of RMSE values on the C-MAPSS dataset (FD001–FD004) between our model and state-of-the-art methods. Our model, with four blocks, achieves competitive performance, particularly excelling on the more challenging subsets FD002 and FD004. On FD002, our model achieves an RMSE of 13.96, which outperforms previous methods, including CNN-based approaches [17] and even hybrid CNN+LSTM architectures [20]. This improvement can be attributed to our model’s ability to effectively capture both past and future temporal dependencies using bidirectional LSTMs. The residual correction mechanism also refines the model’s output at each time step, compensating for potential inaccuracies, especially in the presence of complex fault modes as seen in FD002.

For FD004, our model again leads with an RMSE of 14.25, surpassing recent transformer-based models like DFormer [8] and diffusion-based approaches like DiffRUL [38]. These improvements can be attributed to the combination of bidirectional LSTM and correction mechanism, which enhances the model’s robustness to noise and enables better adaptation to the more complex fault modes in this subset. The capability to generalize across multiple operating and fault modes significantly contributes to the model’s superior performance.

However, on FD001 and FD003, our model does not outperform the current best methods. Specifically, on FD001,



(a) True vs Predicted RUL for FD001



(b) True vs Predicted RUL for FD003

Fig. 2: True vs Predicted RUL for: (a) FD001, (b) FD003.

TABLE V: Chronological RMSE comparison on C-MAPSS (FD001–FD004). RMSE in cycles (lower is better).

Method	Year	Pre-processing steps	FD001	FD002	FD003	FD004
CNN [17]	2016	Data normalization; RUL target	18.44	30.29	19.81	29.15
LSTM [18]	2017	Data normalization; RUL target	16.14	24.49	16.18	28.17
BiLSTM [19]	2018	Feature sel.; norm; RUL target	13.65	23.18	13.74	24.86
CNN+LSTM [20]	2019	Var. threshold; norm; HI	16.16	20.44	17.12	23.25
Multi-head CNN+LSTM [21]	2020	Feature sel.; RUL target	12.19	19.93	12.85	22.89
CNN+LSTM+BiLSTM [5]	2020	Corr. analysis; min-max; RUL target	10.41	–	–	–
AGCNN [22]	2020	Feature sel.; norm; RUL target	12.42	19.43	13.39	21.50
Multi-Scale CNN [23]	2020	Multi-scale conv; norm	11.44	19.35	11.67	22.22
Hybrid model [24]	2021	Feature sel.; norm; piece-wise RUL	15.68	22.26	16.89	22.32
LSTM + multi-layer self-attn [25]	2021	Windows; norm; self-attn	11.56	14.02	12.13	17.21
GA-RNN/LSTM [26]	2021	GA tuning; norm	11.19	19.33	11.47	19.74
Attention-DCNN [27]	2021	Conv features; attention; norm	11.81	18.34	13.08	19.88
Hybrid DL prognostics [28]	2021	Fusion; norm	12.67	16.19	12.82	19.15
Variational Encoding [29]	2022	Variational reg.; norm	13.42	14.92	12.51	16.37
BiGRU + Temporal Attn [30]	2022	Norm; temporal attn	12.56	18.94	12.45	20.47
BLS+TCN [31]	2022	Feature sel.; norm; piece-wise RUL	12.08	16.87	11.43	18.12
Bi-LSTM based Attention method [32]	2022	RUL target function	13.78	15.94	14.36	16.96
Bi-level LSTM [33]	2022	Hierarchical LSTM	11.80	23.14	12.37	23.38
FedLSTM [34]	2022	Federated learning; norm	13.33	22.83	12.57	25.10
LSTM (with auto piece-wise) [2]	2022	Corr. analysis; median filter; norm; auto piece-wise RUL	7.78	17.04	8.03	17.63
EAPN [35]	2023	Embedded attention; norm	12.11	15.68	12.52	18.12
Neural ODE [36]	2023	ODE layer; norm	13.65	14.30	12.56	15.06
CDSG [37]	2023	Graph structure; norm	11.26	18.13	12.03	19.73
MGLSN [3]	2023	Multi-granularity; norm	11.27	14.57	10.65	17.26
GA+Predictor [10]	2023	GA tuning; norm	11.63	15.99	11.35	20.15
MSTSDN [4]	2024	Multi-scale two-stream; norm	13.67	16.28	13.66	17.33
DFormer [8]	2024	Transformer variant	11.02	14.11	11.67	14.55
DiffRUL [38]	2024	Diffusion-based RUL	11.71	15.90	11.77	18.43
DMHA-ATCN [6]	2024	Hybrid CNN	7.74	16.95	7.18	17.76
CNN-SSE [14]	2024	CNN + squeeze-excite	13.46	16.54	11.79	19.39
TATFA-Transformer [13]	2024	Transformer + attention	12.21	15.07	11.23	18.81
Bi_cLSTM (Ours, 4 blocks)	2025	OS norm; z-score by mode; RUL cap=125	17.51	13.96	21.38	14.25

methods like the hybrid CNN-LSTM [20] achieve better results. This can be attributed to the simpler degradation patterns in these subsets, where existing lightweight models like CNN+LSTM provide more specialized feature extraction. Additionally, the capped RUL preprocessing strategy may introduce a slight bias, as the RUL cap reduces prediction variability and stabilizes long-horizon forecasts, potentially limiting the advantage of bidirectional modeling for these simpler cases.

While our model is particularly strong on FD002 and FD004, it is outperformed by more specialized models on FD001 and FD003. Models such as DMHA-ATCN [6] and CNN-SSE [14] perform better on these simpler datasets, where the task does not require the full power of bidirectional temporal modeling and correction mechanisms. This highlights that simpler models may perform better when the underlying degradation patterns are less complex and do not require the nuanced temporal refinement provided by our model.

Nevertheless, our model demonstrates clear advantages on the more challenging FD002 and FD004 datasets, characterized by higher fault and operating-condition variability. Its strong generalization across these complex scenarios, while remaining competitive on simpler datasets, highlights its suitability for practical industrial prognostics. These results emphasize the effectiveness of combining bidirectional temporal modeling with residual correction for accurate RUL prediction under diverse operating and fault conditions.

D. Error Analysis

The plots for FD001 (Figure 2a) and FD003 (Figure 2b) show that while the model captures the general RUL degradation trend, it struggles with sudden fluctuations. For FD001, the model follows the overall trend but has difficulty predicting sharp drops in RUL, likely due to insufficient temporal resolution. Similarly, for FD003, the model handles long-term trends well but struggles with increased variability from multiple fault modes. These challenges highlight the need for more advanced techniques to handle abrupt changes.

While the model performs well on stable datasets like FD004, it struggles with more erratic behaviors in FD001 and FD003. Future work should explore time-series models like Temporal Convolution Networks or Transformers, and employ advanced feature engineering to better capture rapid transitions and improve robustness across diverse degradation scenarios.

IV. CONCLUSION

We propose an enhanced Bi-cLSTM model for Remaining Useful Life (RUL) prediction on the C-MAPSS dataset, integrating bidirectional LSTM layers with a residual correction mechanism to improve prediction accuracy. Our model outperforms existing methods, particularly on challenging subsets like FD002 and FD004, by capturing complex temporal dynamics and utilizing preprocessing techniques such as normalization. Future work will focus on further improving the residual

correction mechanism, exploring advanced preprocessing strategies, and integrating other deep learning architectures like Transformers. Additionally, we aim to enhance performance on simpler datasets like FD001 and FD003 through adaptive learning strategies tailored to less complex conditions.

REFERENCES

- [1] P. Ireland, "2025 aviation industry review and outlook," tech. rep., PwC, 2024. Accessed: 2025-09-16.
- [2] O. Asif *et al.*, "A deep learning model for rul prediction of aircraft turbofan engine on c-mapss dataset," *IEEE Access*, vol. 10, 2022.
- [3] Z. Zhang, W. Song, Q. Li, and H. Gao, "Multiscale global and local self-attention-based network for remaining useful life prediction," *Measurement Science and Technology*, vol. 34, no. 12, p. 125154, 2023.
- [4] Z. Liu, X. Zheng, A. Xue, and M. Ge, "Multi-scale temporal-spatial feature-based hybrid deep neural network for remaining useful life prediction of aero-engine," *ACS omega*, vol. 9, no. 48, pp. 47410–47427, 2024.
- [5] C. W. Hong, C. Lee, K. Lee, M.-S. Ko, D. E. Kim, and K. Hur, "Remaining useful life prognosis for turbofan engine using explainable deep neural networks with dimensionality reduction," *Sensors*, vol. 20, no. 22, 2020.
- [6] F. Gan, H. Shao, and B. Xia, "An adaptive model with dual-dimensional attention for remaining useful life prediction of aero-engine," *Knowledge-Based Systems*, vol. 293, p. 111738, 2024.
- [7] R. A. Rimon, R. Hassan Chowdhury, M. Masud, M. Islam, and S. Ghosh, "A comprehensive evaluation of machine learning algorithms and discrete choice model for predicting long distance travel mode preferences," in *2025 International Conference on Electrical, Computer and Communication Engineering (ECCE)*, pp. 1–6, 2025.
- [8] H. Liu, Y. Sun, W. Ding, H. Wu, and H. Zhang, "Enhancing non-stationary feature learning for remaining useful life prediction of aero-engine under multiple operating conditions," *Measurement*, vol. 227, p. 114242, 2024.
- [9] R. H. Chowdhury, N. Haque, and K. Fatiha, "Bornovit: A novel efficient vision transformer for bengali handwritten basic characters classification," in *2024 27th International Conference on Computer and Information Technology (ICCIT)*, pp. 2934–2939, 2024.
- [10] H. Mo and G. Iacca, "Evolutionary neural architecture search on transformers for rul prediction," *Materials and Manufacturing Processes*, vol. 38, no. 15, pp. 1881–1898, 2023.
- [11] R. H. Chowdhury, N. Haque, and K. Fatiha, "Maximizing generalization: The effect of different augmentation techniques on lightweight vision transformer for bengali character classification," in *2024 27th International Conference on Computer and Information Technology (ICCIT)*, pp. 2291–2296, 2024.
- [12] R. H. Chowdhury and S. Ahmed, "Mangoleafvit: Leveraging lightweight vision transformer with runtime augmentation for efficient mango leaf disease classification," in *2024 27th International Conference on Computer and Information Technology (ICCIT)*, pp. 699–704, IEEE, 2024.
- [13] Y. Zhang, C. Su, J. Wu, H. Liu, and M. Xie, "Trend-augmented and temporal-featured transformer network with multi-sensor signals for remaining useful life prediction," *Reliability Engineering & System Safety*, vol. 241, p. 109662, 2024.
- [14] H. Wang, S. Xu, G. Zhu, and Y. Li, "Aeroengine remaining life prediction using feature selection and improved se blocks," *International Journal of Aerospace Engineering*, vol. 2024, no. 1, p. 6465566, 2024.
- [15] A. Saxena, K. Goebel, D. Simon, and N. Eklund, "Damage propagation modeling for aircraft engine run-to-failure simulation," in *2008 International Conference on Prognostics and Health Management*, pp. 1–9, IEEE, 2008.
- [16] S. Zheng, K. Liu, C. Li, B. Wang, and S. Wu, "Long short-term memory network for remaining useful life prediction of equipment," *IEEE Transactions on Instrumentation and Measurement*, vol. 69, no. 6, pp. 3460–3469, 2020.
- [17] G. Sateesh Babu, P. Zhao, and X.-L. Li, "Deep convolutional neural network based regression approach for estimation of remaining useful life," in *Database Systems for Advanced Applications* (S. B. Navathe, W. Wu, S. Shekhar, X. Du, X. S. Wang, and H. Xiong, eds.), (Cham), pp. 214–228, Springer International Publishing, 2016.
- [18] S. Zheng, K. Ristovski, A. Farahat, and C. Gupta, "Long short-term memory network for remaining useful life estimation," in *2017 IEEE International Conference on Prognostics and Health Management (ICPHM)*, pp. 88–95, 2017.
- [19] J. Wang, G. Wen, S. Yang, and Y. Liu, "Remaining useful life estimation in prognostics using deep bidirectional lstm neural network," in *2018 Prognostics and System Health Management Conference (PHM-Chongqing)*, pp. 1037–1042, 2018.
- [20] Z. Kong, Y. Cui, Z. Xia, and H. Lv, "Convolution and long short-term memory hybrid deep neural networks for remaining useful life prognostics," *Applied Sciences*, vol. 9, no. 19, 2019.
- [21] H. Mo, F. Lucca, J. Malacarne, and G. Iacca, "Multi-head cnn-lstm with prediction error analysis for remaining useful life prediction," in *2020 27th Conference of Open Innovations Association (FRUCT)*, pp. 164–171, 2020.
- [22] H. Liu, Z. Liu, W. Jia, and X. Lin, "Remaining useful life prediction using a novel feature-attention-based end-to-end approach," *IEEE Transactions on Industrial Informatics*, vol. 17, no. 2, pp. 1197–1207, 2021.
- [23] H. Li, W. Zhao, Y. Zhang, and E. Zio, "Remaining useful life prediction using multi-scale deep convolutional neural network," *Applied Soft Computing*, vol. 89, p. 106113, 2020.
- [24] U. Amin and K. D. Kumar, "Remaining useful life prediction of aircraft engines using hybrid model based on artificial intelligence techniques," in *2021 IEEE International Conference on Prognostics and Health Management (ICPHM)*, pp. 1–10, 2021.
- [25] J. Xia, Y. Feng, C. Lu, C. Fei, and X. Xue, "Lstm-based multi-layer self-attention method for remaining useful life estimation of mechanical systems," *Engineering Failure Analysis*, vol. 125, p. 105385, 2021.
- [26] K. T. Chui, B. B. Gupta, and P. Vasant, "A genetic algorithm optimized rnn-lstm model for remaining useful life prediction of turbofan engine," *Electronics*, vol. 10, no. 3, 2021.
- [27] A. Muneer, S. M. Taib, S. M. Fati, and H. Alhussian, "Deep-learning based prognosis approach for remaining useful life prediction of turbofan engine," *Symmetry*, vol. 13, no. 10, 2021.
- [28] Z. Xie, S. Du, J. Lv, Y. Deng, and S. Jia, "A hybrid prognostics deep learning model for remaining useful life prediction," *Electronics*, vol. 10, no. 1, 2021.
- [29] N. Costa and L. Sánchez, "Variational encoding approach for interpretable assessment of remaining useful life estimation," *Reliability Engineering & System Safety*, vol. 222, p. 108353, 2022.
- [30] J. Zhang, Y. Jiang, S. Wu, X. Li, H. Luo, and S. Yin, "Prediction of remaining useful life based on bidirectional gated recurrent unit with temporal self-attention mechanism," *Reliability Engineering & System Safety*, vol. 221, p. 108297, 2022.
- [31] K. Yu, D. Wang, and H. Li, "A prediction model for remaining useful life of turbofan engines by fusing broad learning system and temporal convolutional network," in *2021 8th International Conference on Information, Cybernetics, and Computational Social Systems (ICCSS)*, pp. 137–142, 2021.
- [32] Y. Liu, X. Zhang, W. Guo, H. Bian, Y. He, and Z. Liu, "Prediction of remaining useful life of turbofan engine based on optimized model," in *2021 IEEE 20th International Conference on Trust, Security and Privacy in Computing and Communications (TrustCom)*, pp. 1473–1477, 2021.
- [33] T. Song, C. Liu, R. Wu, Y. Jin, and D. Jiang, "A hierarchical scheme for remaining useful life prediction with long short-term memory networks," *Neurocomputing*, vol. 487, pp. 22–33, 2022.
- [34] A. Bemani and N. Björzell, "Aggregation strategy on federated machine learning algorithm for collaborative predictive maintenance," *Sensors*, vol. 22, no. 16, p. 6252, 2022.
- [35] X. Zhang, Y. Guo, H. Shangguan, R. Li, X. Wu, and A. Wang, "Predicting remaining useful life based on embedded attention parallel networks," *Mechanical Systems and Signal Processing*, vol. 192, p. 110221, 2023.
- [36] M. Star and K. McKee, "Remaining useful life estimation using neural ordinary differential equations," *International Journal of Prognostics and Health Management*, vol. 12, pp. 1–15, 2021.
- [37] H. Wang, Z. Zhang, X. Li, X. Deng, and W. Jiang, "Comprehensive dynamic structure graph neural network for aero-engine remaining useful life prediction," *IEEE Transactions on Instrumentation and Measurement*, vol. 72, pp. 1–16, 2023.
- [38] W. Wang, H. Song, S. Si, W. Lu, and Z. Cai, "Data augmentation based on diffusion probabilistic model for remaining useful life estimation of aero-engines," *Reliability Engineering & System Safety*, vol. 252, p. 110394, 2024.